Induced Freezing of Supercooled Water into Ice by Self-Assembled Crystalline Monolayers of Amphiphilic Alcohols at the Air-Water Interface†

R. Popovitz-Biro,* J. L. Wang, J. Majewski, E. Shavit, L. Leiserowitz,* and M. Lahav*

Contribution from the Department of Materials and Interfaces, The Weizmann Institute of Science, Rehovot 76100, Israel

Received June 17, 1993. Revised Manuscript Received November 3, 1993•

Abstract: The induced freezing of drops of supercooled water covered by uncompressed monolayers of the aliphatic alcohols $C_nH_{2n+1}OH$, $n = 16$–31 was investigated. The ice-nucleation temperatures were found to depend on the length of the hydrocarbon chain and the parity of the number of carbon atoms in the chain. A gradual increase of the freezing point from −14 °C leveling off to a plateau at −7.5 °C from $n = 22$ onward was observed for the even series. Alcohols with n odd raised the freezing temperature from −11 to −1 °C for $n = 17$–31. Fatty acids ($C_nH_{2n+1}COOH$) or alcohols bearing a fluorocarbon chain or a steroidal backbone as the hydrophobic part induced nucleation of ice at much lower temperatures. Powder X-ray diffraction measurements showed that the monolayer $C_{31}H_{63}OH$ induced formation of hexagonal ice with its (001) face parallel to the monolayer surface. Grazing incidence X-ray diffraction (GID) studies of uncompressed monolayers of $C_nH_{2n+1}OH$ with $n = 16$, 20, 23, 30, 31 on water at 5 °C revealed two-dimensional (2D) crysalline self assembly and yielded their packing arrangements to near atomic resolution.[1] The extent of 2D crystalline order (i.e. coherence length) and the amount of crystalline material were less for monolayers with $n = 16$ and 20 than for monolayers with $n = 23$, 30, 31 according to a GID analysis, the latter property being independently confirmed by FT-IR. The best lattice match to ice was for $n = 30$ and 31, the lattice match to ice being poorer for $n = 20$ and 16, in terms of area per molecule, correlating with their less efficient ice-nucleation behavior. The packing arrangements of the hydrocarbon chains of monolayers $C_{30}H_{61}OH$ and $C_{31}H_{63}OH$ are very similar, but for the orientation of their CH_2OH moieties, which are different, resulting in different ice-nucleation behavior. Further evidence for the role played by the orientation of the C–OH group is the ice-nucleating properties of alcohols $CH_3(CH_2)_nCOX(CH_2)_mOH$ (X = O, NH). In these systems the freezing point was found to depend on the parity of m but not on n. The 2D crystal structures of two ester–alcohols $n = 19$, $m = 9$, 10 on water were determined by GID and lattice energy calculations.[1] Finally, mixtures of aliphatic alcohols with different chain lengths (by up to four CH_2 groups) substantially reduced the ice-nucleation temperature, implying drastic reduction in the lateral order of the 2D nets of alcohol OH groups. On the other hand, up to 50% fluorocarbon alcohol in a mixture with hydrocarbon alcohol did not reduce the freezing temperature of ice, indicating phase separation of crystalline domains.

Introduction

Although ice melts at 0 °C, pure water can be supercooled in a clean atmosphere to temperatures below −30 °C. In order to overcome the free energy barrier to the liquid–solid phase transition the presence of a catalyst for crystal nucleation is necessary. Certain inorganic,[2,3] organic,[4-7] and biological[8-10] materials possess the ability to promote ice nucleation. However, the detailed mechanisms by which these auxiliaries act are not clear. The existence of structured vicinal water near interfaces and its importance in heterogenous ice nucleation have been recognized long ago.[11-14] It has been suggested that ice-nucleating substrates bear surfaces that match the crystal structure of ice and thus serve as templates that induce nucleation by epitaxy.[2,7,15] Another mechanism which invokes the presence of local electric fields that are capable of aligning water molecules into ice-like embryos has been proposed.[16-18] In order to unravel the complexity of this transformation, we designed experiments, using Langmuir layers, aiming at a demonstration of the validity of the first-mentioned mechanism.[19] It has been previously demonstrated that one may design Langmuir monolayers composed of amphiphilic molecules which, in their compressed or uncompressed states, act as templates for induced crystal nucleation at the air–solution interface.[20-23] Amphiphilic molecules forming the

† Dedicated to Sir John Meurig Thomas on his 60th birthday.

• Abstract published in *Advance ACS Abstracts,* January 1, 1994.

(1) Wang, J. L.; Levellier, F.; Jacquemain, D.; Kjaer, K.; Als-Nielsen, J.; Lahav, M.; Leiserowitz, L. *J. Am. Chem. Soc.*, following paper in this issue.
(2) Bryant, G. W.; Hallett, J.; Mason, B. J. *J. Phys. Chem. Solids* **1959**, *12*, 189.
(3) Davis, B. L.; Johnson, L. R.; Moeng, F. J. *J. Appl. Meteorol.* **1975**, *14*, 891.
(4) Langer, G.; Rosinski, J.; Bernsen, S. *J. Atmos. Sci.* **1963**, *20*, 557.
(5) Parungo, F. P.; Lodge, J. P. *J. Atmos. Sci.* **1967**, *24*, 274.
(6) Barthakur, N.; Maybank, D. J. *Nature* **1963**, *200*, 866.
(7) Fukuta, N.; Mason, B. J. *J. Phys. Chem. Solids* **1963**, *24*, 715.
(8) Levin, Z.; Yankofsky, S. A.; Pardes, D.; Magal, N. *J. Clim. Appl. Meteorol.* **1987**, *26*, 1188.
(9) Green, R. L.; Warren, G. J. *Nature* **1985**, *317*, 645.
(10) Caple, G.; Sands, D. C.; Layton, R. G.; Zucker, W. V.; Sneider, J. R. *J. Theor. Biol.* **1986**, *119*, 37.
(11) Drost-Hansen, W.; Lin Singleton, J. *Chemistry of the Living Cell*; JAI Press Inc.: 1991; Vol. 3A, pp 157–180 and references therein.
(12) Fletcher, N. H. *The Chemical Physics of Ice*; Cambridge University Press: Cambridge, U.K., 1970; and references therein.
(13) Klier, K.; Zettlemoyer, A. C. *J. Colloid Interface Sci.* **1977**, *58*, 216.
(14) Hillig, W. B. In *Growth and Perfection of Crystals*; Doremus, R. H., Roberts, B. W., Turnbull, D., Eds.; John Wiley and Sons: New York, 1958; pp 350.
(15) Thangaraj, K.; Palanisamy, M.; Gobinathan, R.; Ramasamy, P. *J. Mater. Sci. Lett.* **1986**, *5*, 326.
(16) Pruppacher, H. R.; Pflaum, J. C. *J. Colloid Interface Sci.* **1975**, *52*, 543.
(17) Shichiri, T.; Nagata, T. *J. Cryst. Growth* **1981**, *54*, 207.
(18) Gavish, M.; Wang, J.-L.; Eisenstein, M.; Lahav, M.; Leiserowitz, L. *Science* **1992**.
(19) Gavish, M.; Popovitz-Biro, R.; Lahav, M.; Leiserowitz, L. *Science* **1990**, *250*, 973.
(20) Landau, E. M.; Grayer Wolf, S.; Levanon, M.; Leiserowitz, L.; Lahav, M.; Sagiv, J. *J. Am. Chem. Soc.* **1989**, *111*, 1436.
(21) Weissbuch, I.; Berkovic, G.; Leiserowitz, L.; Lahav, M. *J. Am. Chem. Soc.* **1990**, *112*, 5874.
(22) Landau, E. M.; Popovitz-Biro, R.; Levanon, M.; Leiserowitz, L.; Lahav, M. *Mol. Cryst. Liq. Cryst.* **1986**, *134*, 323.
(23) Mann, S.; Heywood, B. R.; Rajam, S.; Birchall, J. D. *Nature* **1988**, *334*, 692.

0002-7863/94/1516-1179$04.50/0

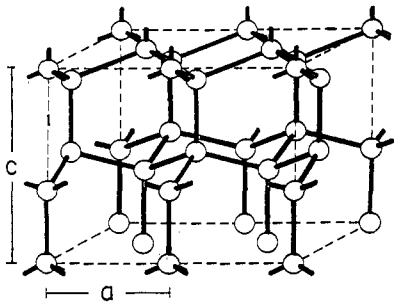

Figure 1. Crystal structure of hexagonal ice.[25,26] The oxygen atoms are denoted by spheres and the disordered O–H···O bonds by rods.

Langmuir layer may be designed such that their hydrophilic head groups will create a surface or a template similar to a layer of the to-be-nucleated crystal. Furthermore, by modifying the hydrophobic tail, it is possible to vary, albeit within limits, the packing arrangement of the head groups and, consequently, directly influence the kinetics of crystal nucleation as well as the type of face of the crystal nucleated under the monolayer.

Direct structural information on such two-dimensional nuclei from which crystals start to grow can be obtained by grazing incidence X-ray diffraction measurements (GID).[24] Such a strategy may provide a structure–function correlation, on a molecular level, as to the mechanism responsible for ice nucleation.

The stable form of ice (ice I), crystallized under atmospheric pressure, is hexagonal[25,26] (Figure 1), space group $P6_3/mmc$, with axes $a = b = 4.5$ Å, $c = 7.3$ Å, $\gamma = 120°$. The crystal structure may be described, in terms of the oxygen atoms, as composed of bilayers 0.9 Å thick parallel to the *ab* plane and separated by 2.75 Å along the hexagonal *c* axis. The axial length of 4.5 Å in the *ab* plane is the separation distance between two water molecules, both hydrogen bonded to the same water molecule within the bilayer. Each oxygen atom participates in three O–H···O hydrogen bonds within the bilayer and a fourth O–H···O bond of 2.75 Å interlinking the neighboring bilayers. The area per molecule of water within an *ab* layer is $a^2 \sin 120° = 17.5$ Å^2.

A grazing incidence X-ray diffraction pattern of the *compressed* monolayer of alcohol $C_{21}H_{43}OH$ on water at 0 °C has been measured.[27] The deduced unit cell may, to a first approximation, be regarded as *c*-centered rectangular with dimensions $a = 5.0$ Å and $b = 7.42$ Å (Figure 2). For the purpose of comparison with the unit cell of ice, we may represent this cell in terms of a distorted hexagonal $a_h = b_h = 0.5(a \pm b) = 4.5$ Å, $\gamma_h = 113°$. It had already been demonstrated with a variety of systems, that amphiphilic molecules tend to self-aggregate into two-dimensional crystalline clusters.[24,28] We therefore anticipated that long-chain aliphatic alcohols may also form crystalline self assemblies and so function as promoters of ice nucleation, from which preliminary results have been reported.[19]

Results

Ice Nucleation under Monolayers of Aliphatic Alcohols. The activity of these alcohol monolayes as ice nucleators was evaluated by measuring the threshold freezing temperatures of supercooled water drops (10 μL) covered by the monolayers and was compared to that of drops covered by monolayers of the corresponding carboxylic acids, for which we do not expect a structural match. In this way, all factors responsible for ice nucleation, other than a difference in the structural match of the two monolayers to ice, were elimianted. Freezing point measurements were carried out

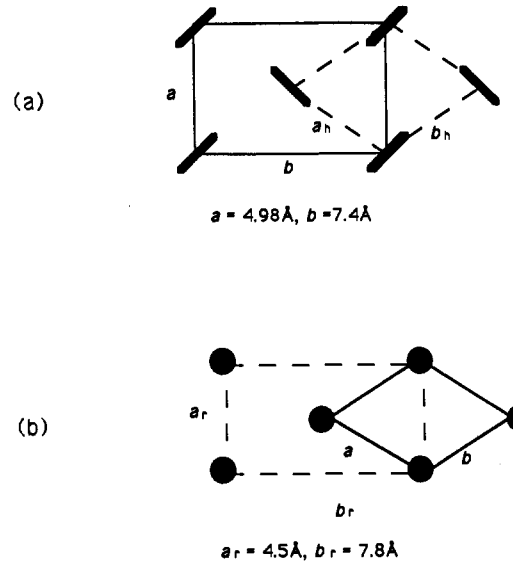

Figure 2. (a) Schematic representation of the orthogonal packing O⊥ of hydrocarbon chains of an alcohol monolayer in a rectangular cell (*a*, *b*), viewed along the chain axis. The distorted hexagonal representation (a_h, b_h) is also depicted. (b) Schematic representation of hexagonal ice in terms of the hexagonal cell (*a*, *b*) and the *c*-centered rectangular cell (a_r, b_r).

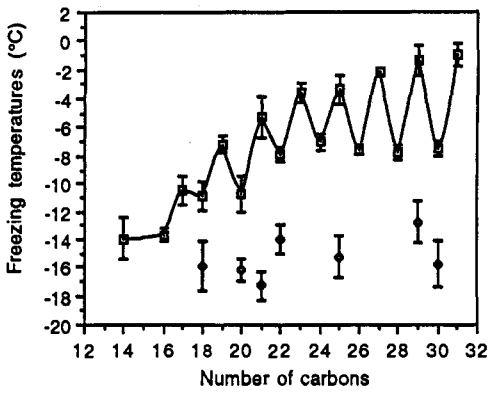

Figure 3. Freezing temperatures of supercooled water drops covered by monolayers of aliphatic alcohols $C_nH_{2n+1}OH$ (□) and carboxylic acids $C_{n-1}H_{2n-1}CO_2H$ (◇) vs the number of carbon atoms in the chain.

on drops of water covered by aliphatic alcohols $C_nH_{2n+1}OH$ with $n = 14$–31. The area per molecule, as obtained from pressure–area (II–*A*) isotherms, for such alcohols is 18–20 Å^2. The results (Figure 3) show that the aliphatic alcohols nucleate ice at higher temperatures and more reproducibly than the corresponding carboxylic acids. Moreover, freezing points appear to be strikingly sensitive to the length of the aliphatic chain and parity of the number of carbon atoms in the chain. The freezing point curve for the n = odd series increases with chain length, reaching a value of −1 °C for $n = 31$, whereas in the n = even series a plateau at −8 °C is reached for $n = 22$. Freezing temperatures obtained for drops covered by monolayers of the analogous aliphatic carboxylic acids ($C_{n-1}H_{2n-1}CO_2H$) were scattered in the range −12 to −18 °C. Analogous nucleation behavior was obtained when the experiments were carried out on deuterium oxide (mp = +3.8 °C). The freezing point curve for the n = odd series increased with chain length, reaching 1 °C for $n = 31$, and in the n = even series a plateau is reached at −4 °C for $n = 22$ (Figure 4). This trend suggests that, prior to ice nucleation, the orientations or structures of the OH groups in the odd and even analogs are not the same, the former having a better structural match with ice. The effect of increasing the cross-sectional area per molecule was also examined. Perfluorododecanol and cholesterol, which have decidedly larger molecular areas (28 and 38 Å^2, respectively) than the *ab* unit cell of hexagonal ice, were found to be poor nucleators (freezing points = −15 °C).

(24) Jacquemain, D.; Leveiller, F.; Weinbach, S.; Lahav, M.; Leiserowitz, L.; Kjaer, K.; Als-Nielsen, J. *J. Am. Chem. Soc.* **1991**, *113*, 7684–7691.
(25) Pauling, L. *J. Am. Chem. Soc.* **1935**, *57*, 2680.
(26) Peterson, W.; Levy, H. A. *Acta Crystallogr.* **1957**, *10*, 70.
(27) Barton, S. W.; Thomas, B. N.; Flom, E. B.; Rice, S. A.; Lin, B.; Peng, J. B.; Ketterson, J. B.; Dutta, P. *J. Chem. Phys.* **1988**, *89*, 2257.
(28) Jacquemain, D.; Grayer Wolf, S.; Leveiller, F.; Lahav, M.; Leiserowitz, L.; Deutsch, M.; Kjaer, K.; Als-Nielsen, J. *J. Am. Chem. Soc.* **1990**, *112*, 7724.

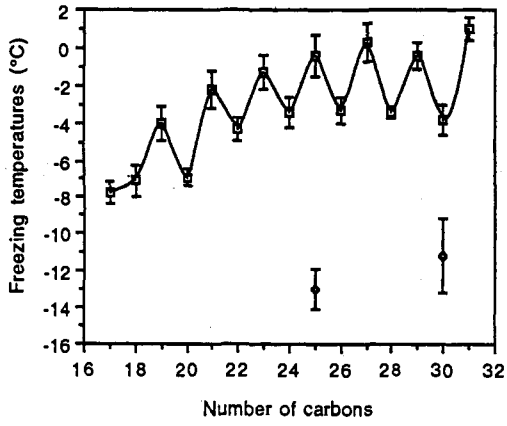

Figure 4. Freezing temperatures of supercooled drops of deuterium oxide covered by monolayers of aliphatic alcohols $C_nH_{2n+1}OH$ (□) and carboxylic acids $C_{n-1}H_{2n-1}CO_2H$ (◇) vs the number of carbon atoms in the chain.

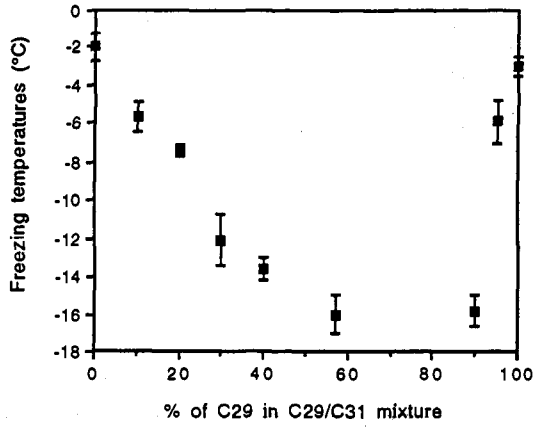

Figure 5. Freezing temperatures of water drops covered by mixed monolayers of alcohols $C_nH_{2n+1}OH$ with n = 29 and 31 in various ratios vs the percentage of $C_{29}H_{59}OH$ in the mixture.

Ice Nucleation under Monolayers of Mixed Aliphatic Alcohols. A strong support for the observation that ice nucleation by the alcohol $C_nH_{2n+1}OH$ monolayers results from specific structural interactions between the monolayer and the nucleating crystal comes from experiments carried out with mixed monolayers. Such monolayers formed from two miscible hydrocarbon alcohols showed typical solid solution behavior. Threshold freezing temperatures of water drops covered by mixed monolayers of aliphatic alcohols with n = 29 and n = 31 in various ratios were lower than the freezing points obtained for each of the pure monolayers (Figure 5). It is noteworthy that there is an asymmetry in the curve of the mixed monolayers. Adding up to 60% of $C_{29}H_{59}OH$ to monolayer $C_{31}H_{63}OH$ gradually reduced the freezing temperature from −1 to −16 °C. On the other hand, only 10% of $C_{31}H_{63}OH$, in a monolayer mixture with $C_{29}H_{59}OH$, was required to reduce the induced freezing temperature from −1.5 to −16 °C in the mixture. In a different experiment, when two alcohols from the n = even series, n = 28 and n = 30, that each induce nucleation at the same temperature (−7.5 °C) when they are pure, were mixed in various ratios, nucleation occurred at much lower temperatures (Figure 6). Similar behavior was observed with mixed monolayers created by mixing two alcohols differing by only one methylene group (n = 30 with n = 31), as shown in Figure 7. This behavior suggests that monolayers of two miscible alcohols create surfaces of hydroxyl groups whose structural fit to ice, as deduced for the pure phases, had been perturbed. This irregularity may result from a surface roughness at the monolayer–water interface due to the difference in their chain length. Similarly, when a monolayer of the aliphatic alcohol with n = 30 was mixed with the corresponding carboxylic acid

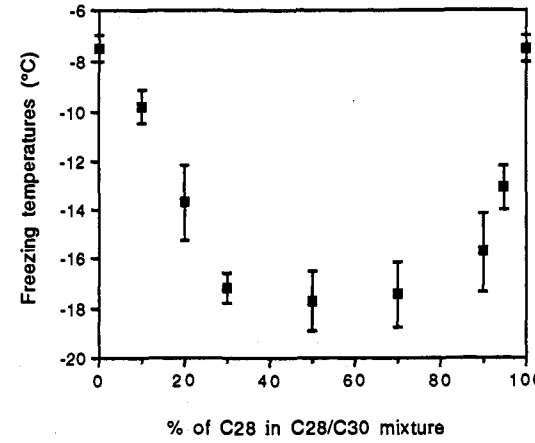

Figure 6. Freezing temperatures of water drops covered by mixed monolayers of alcohols $C_nH_{2n+1}OH$ with n = 28 and 30 in various ratios vs the percentage of $C_{28}H_{57}OH$ in the mixture.

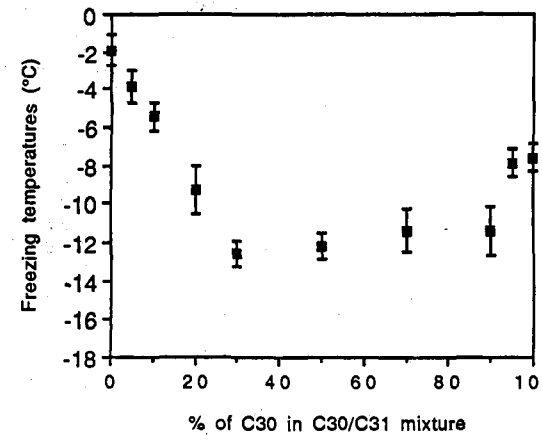

Figure 7. Freezing temperatures of water drops covered by mixed monolayers of alcohols $C_nH_{2n+1}OH$ with n = 30 and 31 in various ratios vs the percentage of $C_{30}H_{61}OH$ in the mixture.

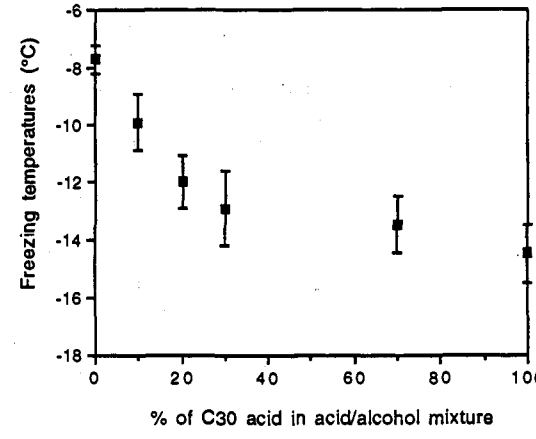

Figure 8. Freezing temperatures of water drops covered by mixed monolayers of the aliphatic alcohol $C_{30}H_{61}OH$ and the corresponding carboxylic acid $C_{29}H_{59}CO_2H$ in various ratios vs the percentage of the acid in the mixture.

which does not nucleate ice, a gradual decrease in freezing temperature was observed (Figure 8).

In contrast to the case of the above systems, when the film is created from an aliphatic alcohol and a perfluorinated one, the two components segregate into immiscible crystalline domains, as indicated by the Π–A isotherms. Up to 50% of $C_{10}F_{21}CH_2$-CH_2OH could be mixed in the monolayer of $C_{20}H_{41}OH$ without perturbing its ice-nucleation activity, as shown in Figure 9.

Ice Nucleation under Monolayers of Alcohols Bearing a Functional Group in the Hydrocarbon Chain. The sensitivty of

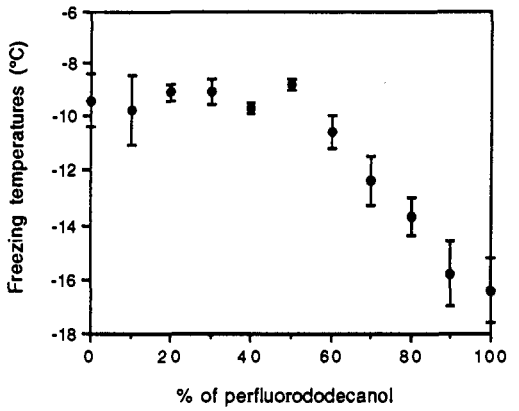

Figure 9. Freezing temperatures of supercooled water drops covered by mixed monolayers of $C_{20}H_{41}OH$ with 1*H*,1*H*,2*H*,2*H*-perfluorododecanol in various ratios vs the percentage of the perfluorinated alcohol in the mixture.

Table 1. Freezing Points of Supercooled Water Drops Covered by Monolayers of Alcohols Bearing an Ester or an Amide Group

	compound	freezing points
1	$CH_3(CH_2)_{10}CO_2(CH_2)_{10}OH$	−4.2 ± 0.6
2	$CH_3(CH_2)_{13}CO_2(CH_2)_9OH$	−10.0 ± 0.8
3	$CH_3(CH_2)_{13}CO_2(CH_2)_{10}OH$	−4.75 ± 0.7
4	$CH_3(CH_2)_{18}CO_2(CH_2)_8OH$	−5.5 ± 0.5
5	$CH_3(CH_2)_{18}CO_2(CH_2)_9OH$	−9.0 ± 0.8
6	$CH_3(CH_2)_{18}CO_2(CH_2)_{10}OH$	−4.0 ± 0.7
7	$CH_3(CH_2)_{18}CO_2(CH_2)_{12}OH$	−4.3 ± 0.9
8	$CH_3(CH_2)_{18}CO_2(CH_2)_{13}OH$	−8.0 ± 0.4
9	$CH_3(CH_2)_{20}CO_2(CH_2)_9OH$	−8.8 ± 0.8
10	$CH_3(CH_2)_{20}CO_2(CH_2)_{10}OH$	−3.0 ± 0.7
11	$CH_3(CH_2)_{10}CONH(CH_2)_{11}OH$	−7.5 ± 0.3
12	$CH_3(CH_2)_{10}CONH(CH_2)_{12}OH$	−3.3 ± 0.5
13	$CH_3(CH_2)_{14}CONH(CH_2)_{11}OH$	−7.4 ± 0.3
14	$CH_3(CH_2)_{14}CONH(CH_2)_{12}OH$	−3.3 ± 0.4
15	$CH_3(CH_2)_{20}CONH(CH_2)_{11}OH$	−7.3 ± 0.8
16	$CH_3(CH_2)_{20}CONH(CH_2)_{12}OH$	−3.8 ± 0.8

ice nucleation to subtle changes in cross-sectional molecular area was further examined by introducing functional groups, such as esters or amides, along the hydrocarbon chain of the alcohols, as shown in Table 1. For such amphiphiles the area per molecule, as obtained from Π–*A* isotherms, are in the range 22–24 Å^2. The ice-nucleation results show no dependence of freezing temperature on length and parity of the number of atoms in the chain. However we can divide the amphiphiles into two groups which nucleate ice at temperatures differing by about 4 °C (Table 1). The structural difference between the two groups is the parity of the number of carbon atoms in the hydrocarbon fragment connecting the functional group to the hydroxyl head group. This behavior suggests that the interactions between the functional groups along the hydrocarbon chain fix the packing arrangement as to influence on the orientation of the OH head group at the interface. Further support for this idea comes from experiments carried out on mixed films of alcohols bearing amide groups situated at different positions along the hydrocarbon chain. When amide **12** was mixed in various ratios with **11**, which is shorter by one methylene group in the hydrocarbon fragment between the amide and the alcohol, the freezing temperature decreased gradually, reaching a minimum for a 1:1 mixture (Figure 10). In contrast, when **12** was mixed with **14**, which is longer by four methylene groups in the hydrocarbon fragment between the amide function and the methyl group, there was almost no change in the freezing temperatures relative to those of the pure compounds (Figure 11). Furthermore, in contrast to the behavior of mixed aliphatic alcohols, when **12** was mixed with an aliphatic alcohol of the same length ($C_{25}H_{51}OH$), there was no effect on freezing temperatures relative to those of the pure monolayers (Figure 12). This behavior indicates that the two monolayers segregate into immiscible domains.

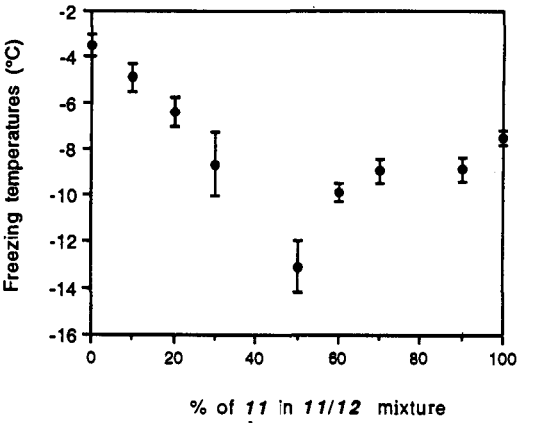

Figure 10. Freezing temperatures of supercooled water drops covered by mixed monolayers of amide–alcohols **11** and **12** in various ratios vs the percentage of **11** in the mixture.

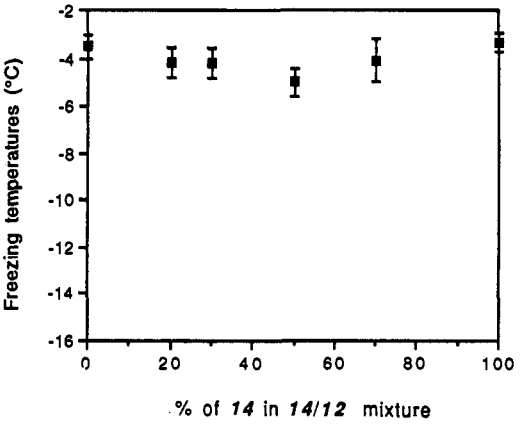

Figure 11. Freezing temperatures of supercooled water drops covered by mixed monolayers of amide–alcohols **12** and **14** in various ratios vs the percentage of **14** in the mixed monolayer.

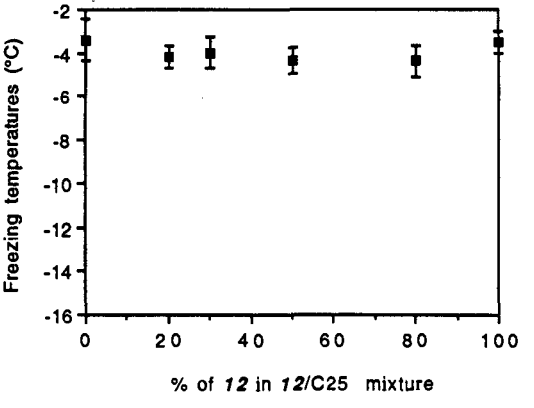

Figure 12. Freezing temperatures of supercooled water drops covered by mixed monolayers of amide–alcohol **12** and the aliphatic alcohol $C_{25}H_{51}OH$ in various ratios vs the percentage of **12** in the mixture.

A different behavior was obtained with mixed monolayers bearing as ester function along the chain. When **10** was mixed in various ratios with **9**, which is shorter by one methylene group in the fragment connecting the ester to the hydroxyl head group, the freezing points decrease gradually, reaching a minimum at a 6:4 ratio (Figure 13). When **10** was mixed in various ratios with **6**, which is shorter by two methylene groups in the fragment between the ester and the methyl group, there was a gradual decrease in the freezing points but to a lesser extent than in the **10** and **9** mixtures (Figure 14).

FT-IR Measurements. External reflection Fourier transform infrared spectroscopy[29] has been used to measure the vibrational

(29) Mitchell, M. L.; Dluhy, R. A. *J. Am. Chem. Soc.* **1988**, *110*, 712.

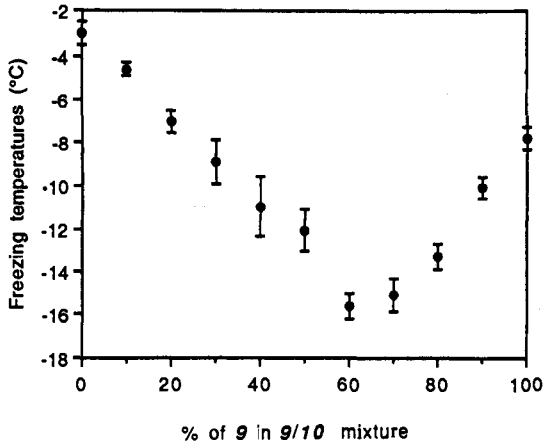

Figure 13. Freezing temperatures of supercooled water drops covered by mixed monolayers of ester–alcohols **9** and **10** in various ratios vs the percentage of **9** in the mixture.

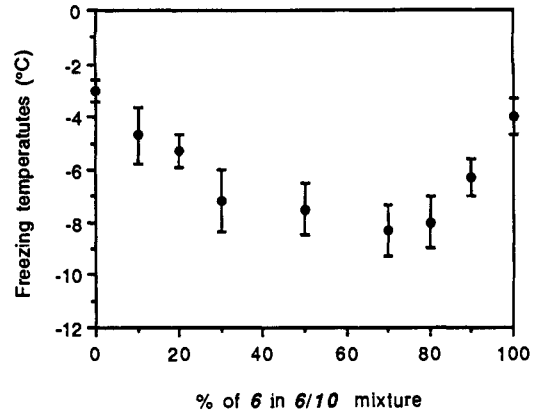

Figure 14. Freezing temperatures of supercooled water drops covered by mixed monolayers of ester–alcohols **6** and **10** in various ratios vs the percentage of **6** in the mixture.

spectra of the aliphatic alcohol monolayers at the air–water interface. The symmetric and antisymmetric stretching frequencies have been shown to be conformation-sensitive[30] and thus may be correlated with the degree of order in the hydrocarbon chain. These stretching vibrations were obtained for the various alcohols $C_nH_{2n+1}OH$ at three different average molecular areas 60, 30, and 20 Å^2 at 20 °C. The ice-nucleation experiments were performed in a complete monolayer surface coverage of the water drops (≈20 Å^2/molecule). Comparison of the IR reflection spectra of the various alcohols at 20 Å^2 shows a shift of 1.0–1.5 cm^{-1} to lower wavenumbers and a decrease of 2–4 cm^{-1} in bandwidth, with increase in chain length from 16 carbons to 30 (Figure 15), suggesting a higher degree of order in the longer alcohols.

X-ray Powder Diffraction Measurements. In order to resolve the questions which face of ice has been nucleated under the monolayer and whether the ice formed is the stable hexagonal form, X-ray powder diffraction measurements were made of ice nucleated under various monolayers in small glass troughs, as described in the Experimental Section. Diffractograms obtained from ice nucleated under a monolayer of alochol $C_{31}H_{63}OH$ indicate preferred orientation of the ice crystals with the *c* axis, corresponding to the hexagonal form, perpendicular to the plane of the sample (Figure 16b). When ice was nucleated in the absence of the monolayer, a randomly oriented ice powder was obtained (Figure 16a). Ice created under a monolayer of $C_{10}F_{21}CH_2CH_2OH$, which does not have a lattice match with the *ab* plane of ice, did not show any preferred orientation of the *c* axis.

(30) Dluhy, R. A.; Cornell, D. G. *Fourier Transform Infrared Spectroscopy in Colloid and Interface Science*; Washington, DC, 1990; Vol. 447, pp 192.

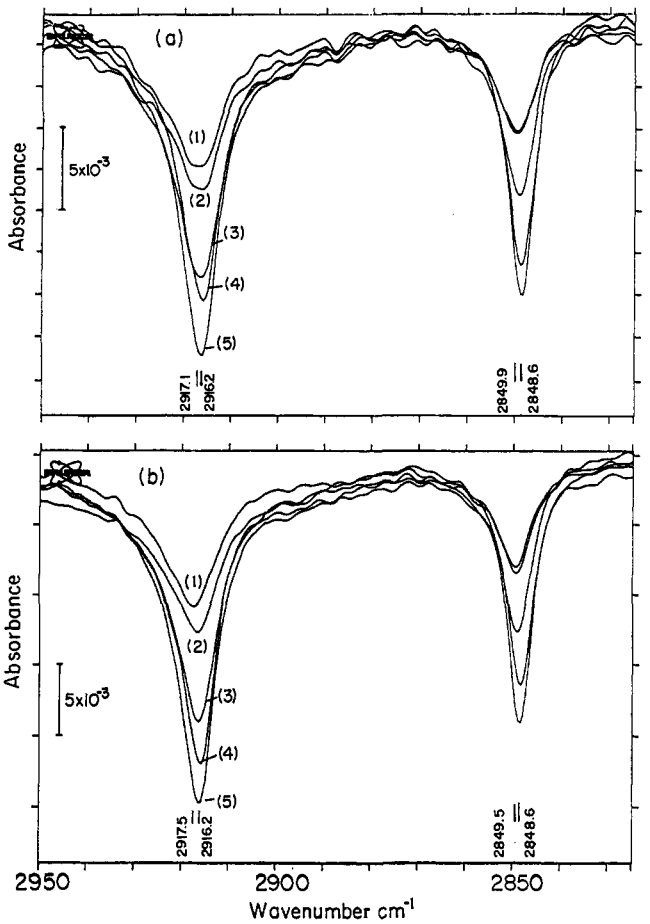

Figure 15. FT–IR external reflection spectra of monolayers of aliphatic alcohols $C_nH_{2n+1}OH$ with (**1**) n = 16, (**2**) n = 19, (**3**) n = 22, (**4**) n = 24, and (**5**) n = 27 on water at 20 °C, showing the hydrocarbon stretching region for (a) parallel and (b) perpendicular polarizations.

Discussion

It is well-known that water-soluble alcohols act as antifreeze agents. Here we have demonstrated that certain water-insoluble species, constrained to the water surface, are efficient ice nucleators. In order to gain understanding, on a molecular level, regarding the structural features influencing epitaxial nucleation of ice, several types of amphiphilic alcohols have been used as ice nucleators and their efficiencies have been correlated with various structural and molecular parameters.

Effect of Molecular Area (Lattice Match) on Ice Nucleation. The area per water molecule in the *ab* layer of hexagonal ice is 17.5 Å^2. Monolayers of alcohols such as perfluorododecanol and cholesterol, which have molecular areas of 28 and 38 Å^2, respectively, do not induce nucleation of ice. The bulky hydrophobic parts of these molecules impose a separation of their hydroxyl groups to a distance larger than 4.5 Å. As mentioned in the introduction, such a distance is favorable for hydrogen bonding of a water molecule to two neighboring hydroxyl groups in a way that is complementary to the structure of ice. Thus in the monolayers containing bulky chains, a lattice or structural match betweeen the monolayer and ice cannot be attained. The highest freezing points were observed with aliphatic alcohols having molecular areas of 18.5–20 Å^2, which are close to the *ab* unit cell area of water in ice. Among this group of aliphatic alcohols, we obtained a large range of ice-nucleating activities which cannot result from the minor changes in molecular area, so requiring that other structural parameters be invoked. Grazing incidence X-ray diffraction (GID) measurements were performed on uncompressed monolayers of $C_nH_{2n+1}OH$, n = 16, 20, 23, 30, 31, over water at 5 °C. The GID patterns of the three monolayers[1,24] n = 23, 30, and 31 are very similar, indicating that

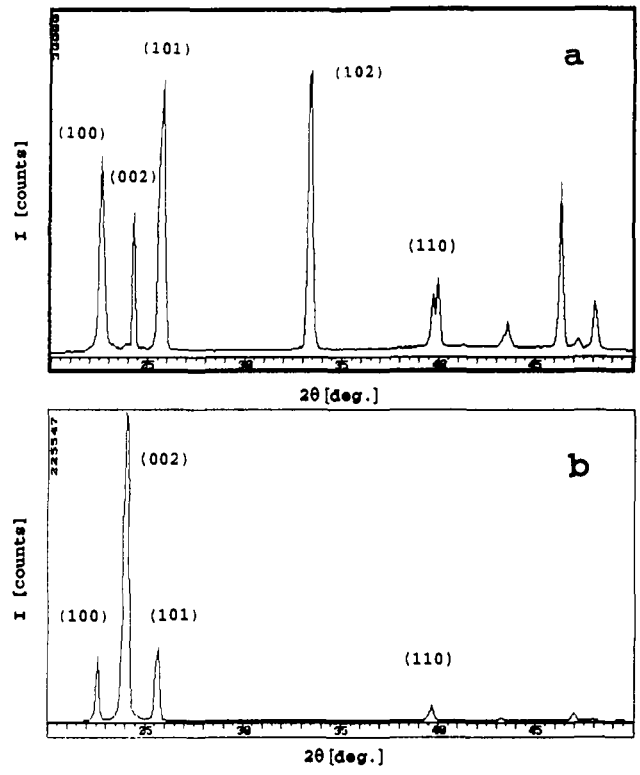

Figure 16. X-ray powder diffractograms (Cu Kα radiation) of (a) ice frozen from pure water and (b) ice nucleated under a monolayer of $C_{31}H_{63}OH$ at 70% surface coverage.

their 2D crystal structures are also very similar. Because of the paucity of the observed GID data, these crystal structures were not determined with the atomic resolution as would be obtained from a 3D molecular crystal. Nevertheless, by making use of information already available from 3D crystal structures of long-chain hydrocarbons, complemented by lattice energy calculations, it was possible to determine, from the GID intensity patterns, the crystal structures of the alcohol monolayers to near-atomic resolution.

We shall confine the description primarily to the $C_{30}H_{61}OH$ and $C_{31}H_{63}OH$ systems, in terms of the GID measurements. Both monolayers are highly crystalline; their coherence lengths, as derived from the widths of the observed Bragg reflections, are anisotropic, in the range 300–1000 Å. Each crystal structure appears in a primitive rectangular unit cell (see Table 2) which contains two molecules related essentially by glide symmetry in the 2D plane group $p1g1$ (The symbol $p1g1$ denotes a primitive (p) unit cell with a glide (g) plane perpendicular to the a axis, the glide being directed along b). The $C_{30}H_{61}OH$ and $C_{31}H_{63}OH$ molecules are tilted from the vertical toward the b axis, between nearest neighbors, by about the same angle of 9° (±1). The area per molecule as projected along the molecular axis, A_p (Table 2), is 18.5 Å^2, which is almost as low as in the densest hydrocarbon lamellar crystals, indicative of a low lateral thermal motion, estimated at root mean square value of 0.3 Å from the GID data. The neighboring hydrocarbon chains are arranged in the herringbone motif, with a dihedral angle of 85° between the planes of the carbon backbone chains, and so denoted as an orthogonal O⊥ motif.[31] The good lattice match between the aliphatic alcohols and ice is revealed by comparing the oxygen positions of the OH head groups in $C_{30}H_{61}OH$ and $C_{31}H_{63}OH$ monolayers with those in the (001) ab layer of ice. The comparison is most easily done by expressing the hexagonal net ($a = b$, $\gamma = 120°$) of ice in terms of a c-centered rectangular cell $a_r = |\mathbf{a} + \mathbf{b}| = 4.5$ Å, $b_r = |\mathbf{b} - \mathbf{a}| = 7.8$ Å, $\gamma_r = 90°$, as shown in Figure 2. The rectangular unit cells of the $C_{30}H_{61}OH$ and $C_{31}H_{63}OH$ crystals are similar in dimensions to the corresponding rectangular c-centered representation ($a_r b_r$) of hexagonal ice, but the plane of symmetry of the alcohol cell is not c-centered but primitive $p1g1$. Nevertheless, the alcohol oxygen atoms lie in a net very close to being c-centered, because the oxygen atoms lie almost halfway, to within 0.3 Å, between neighboring glide planes. Thus we may compare the extent of a lateral match between each of the monolayers of $C_{31}H_{63}OH$ and $C_{30}H_{61}OH$ with the ab lattice structure of ice, by superimposing the 2D nets of their oxygen atom arrangements. There is a reasonable fit over a common area of 600–800 Å^2, corresponding to about 30–40 molecular sites (Figure 17). This common area is much smaller than the area of the crystalline coherence length within either the $C_{30}H_{61}OH$ or $C_{31}H_{63}OH$ monolayers, which is in the range 1000 × 300 Å^2.

The crystal structure determinations of the alcohols with n = 20 and 16 are described here in the Experimental Section. The GID data of these monolayers were different from those with n = 23, 30, and 31, insofar as the molecules are tilted from the vertical by a larger angle of 19° along the b axis, thus leading to an increase in the length of the b axis (Table 2) and so to a poorer lattice match with ice.

The introduction of an amide or ester group along the hydrocarbon chain ($C_nH_{2n+1}COXC_mH_{2m}OH$, X = NH, O) yielded a molecular area of about 22 Å^2. The highest ice-nucleating temperatures obtained with such monolayers were 2–3 °C lower than those for the corresponding aliphatic alcohols. As we shall see later, the monolayer structures of such amphiphiles differ from those of the simple aliphatic alcohols, so that the decrease in nucleation temperature cannot only be correlated with a difference in lattice match to ice but may also result from difference in other structural parameters, such as OH head group orientation at the water interface.

Effect of Chain Length on Ice Nucleation. Among the aliphatic alcohols, we observed an increase in ice-nucleation temperature with a longer chain length. It would seem reasonable that monolayer films of long amphiphiles, $n > 22$, with more methylene–methylene interactions are crystalline, whereas those obtained from the short-chain alcohols tend to be more fluid like.[31] Replacing $C_{20}H_{41}OH$ by $C_{20}D_{41}OH$ in the nucleation experiment resulted in exactly the same freezing temperature, indicating that it is the number of methylene–methylene interactions and not the molecular weight that influences the degree of crystallinity. Indeed, a correlation has been made between the degree of 2D crystallinity and molecular interaction energy for a variety of different amphiphilic molecules on water.[32] For hydrocarbon chains in close contact, their lattice energy contribution is almost proportional to chain length, being ≈2 kcal/mol per CH_2 group. For fatty acid amphiphiles it was also possible to correlate the lateral extent of crystalline coherence with molecular chain length as well as with the angle of tilt of the chain.[33] Such a correlation can also be made for the alcohols according to GID data. The GID measurements on the series $C_nH_{2n+1}OH$, n = 16, 20, 23, 30, 31, indicate that the extent of lateral order (i.e. crystalline coherence length) of these spontaneously formed 2D crystalline clusters decreases with shorter chain length (Table 2). Moreover, as deduced from the widths of their diffraction peaks, this ordering is anisotropic with crystalline coherence lengths ranging from ≈200 to 900 Å in the direction perpendicular to the {1,1} plane and from ≈50 Å (see Experimental Section) for n = 16 (see Experimental Section) to ≈250 Å for n = 31 for the {0,2} plane. The lower coherence length along the {0,2} diffraction vector may be correlated with the fact that the shorter the chain the larger the tilt angle[33] in the b direction. A similar tendency was observed for the monolayers of $C_{29}H_{59}CO_2H$ and $C_{29}H_{59}CO_2C_mH_{2m}OH$ (m = 9,

(31) Small, D. M. *Handbook of Lipid Research*; Plenum Press: 1986; Vol. 4, Chapters 2. 5, and 8.

(32) Jacquemain, D.; Grayer-Wolf, S.; Leveiller, F.; Frolow, F.; Eisenstein, M.; Lahav, M.; Leiserowitz, L. *J. Am. Chem. Soc.* **1992**, *114*, 9983.

(33) Leveiller, F.; Jacquemain, D.; Leiserowitz, L.; Kjaer, K.; Als-Nielsen, J. *J. Phys. Chem.* **1992**, *96*, 10380.

Table 2. Results of the GID Analysis for the Alcohol Monolayers $C_nH_{2n+1}OH$, n = 16, 20, 23, 30, 31, and Ester–Alcohols *5* and *6*[a]

compound	d_{11} (Å) (L)	d_{02} (Å) (L)	d_{20} (Å) (L)	a (Å) (a_p)	b (Å) (b_p)	A (Å^2) A_p	t (deg)	δ (deg)
n = 16[b]	4.21	4.0[c]		4.95[c]	8.0[e]	19.8[e]	19	4.6
	180	low[d]		(5.0)[c]	(7.56)[c]	(18.7)[c]		
	4.21	4.21[e]		4.86[e]	8.41[e]	20.4[e]		
n = 20	4.27	4.00		5.05	8.0	20.2	19	2.4
	700	300		(5.05)	(7.56)	(19.1)		
n = 23	4.18	3.78	2.50	5.00	7.56	18.90	9.5	1.2
	(≥1000)	(360)	(≥1000)	(5.00)	(7.46)	(18.65)		
n = 30	4.15	3.75	2.49	4.99	7.49	18.69	7.7	1.7
	(≥1000)	(230)	(≥1000)	(4.99)	(7.42)	(18.51)		
n = 31	4.16	3.77	2.49	4.99	7.53	18.79	9.7	1.7
	(≥1000)	(270)	(700)	(4.99)	(7.41)	(18.51)		
n = 31[b]	4.15	3.74		4.98	7.45	18.55	5–11	1.5
	850	260		(4.98)	(7.38)	(18.38)		
5	4.57	3.75		5.76	7.50	21.60	30	1.5
	(430)	(≥1000)		(4.99)	(7.50)	(18.71)		
6	4.53	3.74		5.69	7.48	21.28	28	1.8
	(450)	(≥1000)		(5.02)	(7.48)	18.77		

[a] L = coherence length (Å) of the crystallites, determined according to the Scherrer formula. a and b are the lengths (in Å) of the unit cell axes; a_p and b_p are the lengths of the unit cell projected along the molecular chain axis. In these systems $a_p = a$ and $b_p = b \cos t$; in the ester–alcohols, $a_p = a \cos t$ and $b_p = b$. A = area per molecule = $ab/2$. t-tilt angle of monolayer molecules from the normal to the water surface in the b direction for the aliphatic alcohols and in the a direction for *5* and *6*. δ-lean angle of the molecules in the a direction for the aliphatic alcohols and in the b direction for *5* and *6*. [b] These data were measured on beamline BW-1, and the remaining, on beamline D4 (see Experimental Section). The best Bragg rod fitting for an alcohol with n = 31 was obtained by assuming a continuum of chain tilts in the range 5–11°, which was modeled by three tilts of 5°, 8°, and 11° with occupancies of 0.25, 0.5, and 0.25, respectively. [c] The cell dimensions deduced on the basis that the {0,2} reflection was unobserved. [d] Probably ≤50 Å (see text). [e] The cell dimensions deduced on the basis that the {0,2} reflection coincides with the {1,1} + {1,−1} one. Since the {0,2} reflection is much weaker than the {1,1} + {1,−1} one, we safely assume that the observed coherence length of 180 arises primarily from the latter.

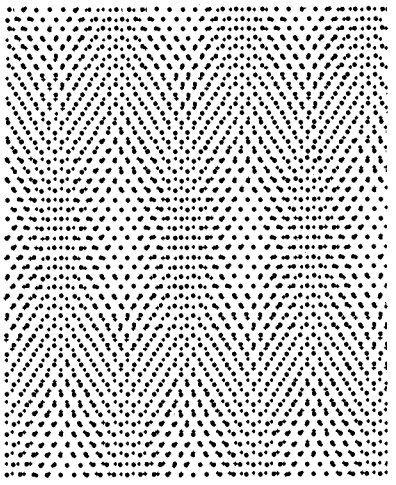

Figure 17. Diagram of the superimposed oxygen positions within the *ab* layer of hexagonal ice (labeled as +) and the oxygen position in a monolayer of $C_{31}H_{63}OH$ (labeled as ·).

10). According to lattice energy calculations performed on these systems,[1] the binding energy of the molecules in the direction of the tilt is distinctly less than the binding energy in the perpendicular direction. Moreover, the amount of crystalline material appears also to be dependent on chain length. According to an analysis of the GID data,[1] the monolayers with n = 23, 30, and 31 contain about the same amount of crystalline material, but monolayers with n = 16 and 20 contain less crystalline material, as described here in the Experimental Section. From IR measurements of long chain hydrocarbons, it has been demonstrated that the frequencies of the antisymmetric and symmetric CH_2 stretching vibrations are conformation-sensitive and may be empirically correlated with order (i.e. the trans–gauche character) of the hydrocarbon chain.[34] External reflectance IR spectra of the aliphatic alcohol $C_nH_{2n+1}OH$ (n = 16, 19, 22, 24, 27) monolayers with an average area per molecule of 20 Å^2 have been measured at the air–water interface at room temperature. In this series there is a shift of 1.0–1.5 cm^{-1} to lower wavenumbers and a decrease of 2–4 cm^{-1} in band width, in both the antisymmetric and symmetric stretching bands with incresae in chain length, indicating that the chains become more ordered (Figure 15).

(34) MacPhail, R. A.; Strauss, H. L.; Snyder, R. G.; Ellinger, C. A. *J. Phys. Chem.* **1984**, *88*, 334.

By and large we may come to the following general conclusion, the longer the chain length of $C_nH_{2n+1}OH$ ($16 \leq n \leq 31$), the greater the amount of crystalline material, the longer the extent of lateral coherence length, and the smaller the tilt angle. Thus it would seem that the more ordered the crystalline domains, the more efficient is the monolayer for ice nucleation. However we should note that the greater the tilt angle (t) of the molecular chain (i.e. $t \approx 9°$ for n = 31 and t = 19° for n = 16), the worse the lattice match to ice in terms of area per molecule, and so degree of crystallinity and lattice match to ice go hand in hand. In order to separate these two effects, we note that the molecular chains of $C_{29}H_{59}CO_2C_mH_{2m}OH$ (m = 9, 10) are highly tilted with $t \approx 26°$ and so exhibit a poorer lattice fit to ice than $C_{16}H_{33}OH$. But monolayers of $C_{29}H_{59}CO_2C_mH_{2m}OH$ have longer coherence lengths than $C_{16}H_{33}OH$ and $C_{20}H_{41}OH$, and are better ice nucleators.

Further evidence for the role played by the extent of lateral order is provided by ice-nucleation and GID experiments carried out with two miscible alcohols $C_{27}H_{55}OH$ and $C_{31}H_{63}OH$. Addition of 5% of $C_{31}H_{63}OH$ as contaminant already reduced the freezing point by about 5 °C. GID measurements have shown that mixed monolayers of $C_{31}H_{63}OH$ and $C_{27}H_{55}OH$ in various proportions form 2D crystalline solid solutions.[1] We may therefore infer that the contaminant molecules are randomly arranged in the monolayer. In such a system the effective coherence length of the OH head groups of the monolayer must be reduced because the OH groups of the contaminant and the host are not arranged in the same manner.

Experiments carried out with mixed monolayers of two immiscible components further demonstrate the effect of the crystalline coherence length on nucleation efficiency. When perfluorododecanol is introduced into a monolayer of an aliphatic alcohol (Figure 9), it seems that crystallinity of the hydrocarbon component was not destroyed and ice-nucleation activity was not perturbed. One possible explanation for this observation is that the gradual increase of perfluorododecanol above 50% causes a reduction in the crystalline domain size of the aliphatic alcohol, which is reflected in the decrease in nucleation efficiency.

Effect of *n* Being Odd or Even in $C_nH_{2n+1}OH$ on Ice Nucleation. Aliphatic alcohols that belong to the group with n = even induce nucleation of ice at temperatures lower than those from the n = odd series, suggesting a systematic structural difference between the films of the two series of alcohols. The hydrocarbon chains

Scheme 1

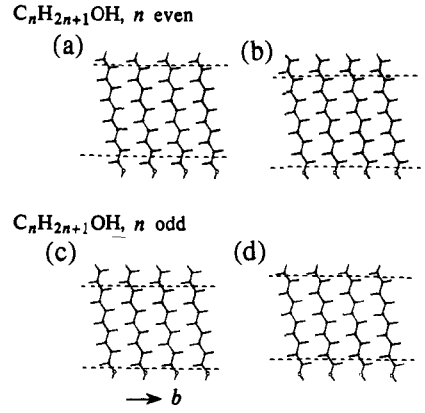

in these two series of alcohol monolayers pack in similar packing arrangements, as exemplified by the GID data of $C_{30}H_{61}OH$ and $C_{31}H_{63}OH$ monolayers. However, there is an ambiguity, which cannot be resolved from the GID data, in fixing the (x,y) positions of the oxygen atoms. Part of the problem arises from the fact that the carbon chain has a regular zig-zag arrangement and so, for a given chain, one cannot differentiate by GID between the two structures shown in Scheme 1a and b even though the (x,y) positions of the oxygen atoms in these two crystal structures are different. This ambiguity manifests itself on comparing the 2D crystal stuctures of $C_{30}H_{61}OH$ and $C_{31}H_{63}OH$. Either the oxygen atoms of the two crystal structures have the same (x,y) coordinates, as in, say, Scheme 1a and c or they do not. Surprisingly, the results of the ice-nucleation experiments allow us to conclude that the oxygen atoms of $C_{30}H_{61}OH$ and $C_{31}H_{63}OH$ are differently positioned. Consequently, the packing of the hydrocarbon chains of $C_{30}H_{61}OH$ and $C_{31}H_{63}OH$ are deduced to be alike from the terminal CH_3 groups down until atoms C(1) and C(2) for the $C_{30}H_{61}OH$ and $C_{31}H_{63}OH$ molecules, respectively. But the ambiguity of which of the two alternative (x,y) positions is adopted by, say, $C_{31}H_{63}OH$ is still unresolved. We have arbitrarily chosen the arrangement shown in Figure 18a for $C_{31}H_{63}OH$. It follows that the $C_{30}H_{61}OH$ crystal structure must have the 'different' arrangement shown in Figure 18b. The intermolecular distances between the oxygen atoms in the 2D crystal structures of $C_{30}H_{61}$-OH and $C_{31}H_{63}OH$ are almost the same (Figure 18c,d). This is because the x coordinates of their oxygen atoms for the two structures, although opposite in sign, are equal in magnitude. In other words, the perpendicular distance of the oxygen atom from the nearest glide plane is almost the same in the two crystal structures.[35]

The molecules adopt an all-trans conformation of the hydrocarbon chains according to the detailed analysis of the GID data for n = 23, 30, and 31. This analysis is also consistent with the chain conformation in the 3D crystal structures of the two long-chain alcohols[36] $C_nH_{2n+1}OH$ of the n even series n = 24 and 16. These molecules form layers in which the chains are titled at an angle of 36° to the layer normal. With such a tilt angle, the hydroxyl group can form geometrically acceptable OH···O hydrogen bonds between layers. In these two 3D crystal stuctures, the hydroxyl oxygen atoms also form part of the all-trans conformation about the C_β–C_α bond. On the other hand, according to the crystal structure[26] of $C_{17}H_{35}OH$, representing molecules $C_nH_{2n+1}OH$ with n odd, the chains are aligned normal to the layer plane, assuming an all-trans conformation of the hydrocarbon segment but with half the number of molecules adopting a trans C_γ–C_β–C_α–OH and the other half a gauche conformation. In this way half of the number of OH···O bonds

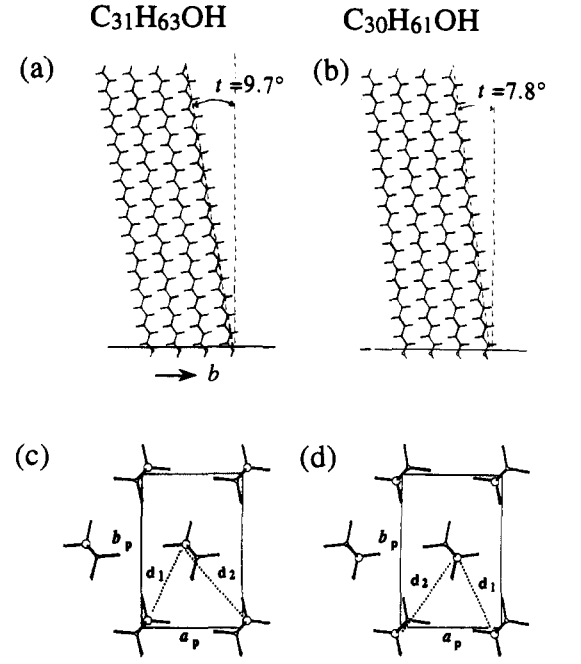

Figure 18. Structure of alcohol monolayers $C_nH_{2n+1}OH$ (n = 30, 31). Parts a and b view along the a axis. Parts c and d view along the molecular chain axis. O···O distances between the glide-related molecules in the unit cell are d_1 = 4.2 Å, d_2 = 4.9 Å for both monolayers. Note that a_p and b_p represent the unit cell axes (a and b) projected onto a plane perpendicular to the molecular chain axis.

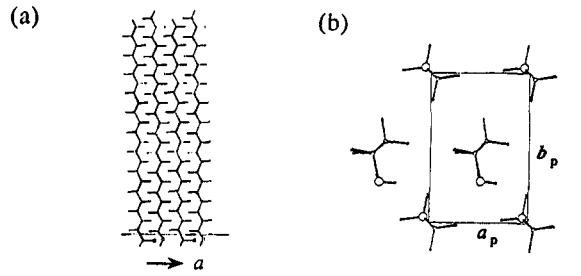

Figure 19. The possible molecular packing arrangements of alcohol monolayers $C_nH_{2n+1}OH$ (n = 30, 31) with half the number of molecules with their C_α–OH groups in the gauche conformation about the C_β–C_α bond. For clarity, a shorter hydrocarbon chain of n = 23 is presented. (a) View along the b axis showing the poor intermolecular contact between the methyl groups at the top of the monolayer. (b) View along the molecular axis.

occur between molecules within layers and the other half between layers. A similar arrangement, shown in Figure 19 was constructed for the $C_{30}H_{61}OH$ and $C_{31}H_{63}OH$ monolayers because the molecules are aligned with a tilt only 9° from the vertical. The model suffers from the disadvantage that the methyl groups of neighboring molecules with different C_γ–C_β–C_α–OH conformations would make poor intermolecular contacts because they differ in height by 1.5 sin(114°/2) = 1.3 Å. Indeed atom–atom potential energy calculations[1] indicated that the all-trans model was preferable, but only marginally so, by ≈ 1.4 kcal/mol. Naturally, it was not possible to rule out the trans–gauche model from the GID data.

Paradoxically, we may also invoke the ice-nucleation experiments to rule out the arrangement (Figure 19) containing the trans and gauche conformations; firstly because the arrangement of OH groups in this motif makes a much worse fit to the (001) ice layer than the arrangement containing only all-trans molecules (Figure 20). Furthermore, the trans–gauche model is inconsistent with the ice-nucleating behavior of the monolayer of the 1:1 mixture of $C_{30}H_{61}OH$ and $C_{31}H_{63}OH$. Such a mixture is ideally suited for the trans–gauche model because the two molecules differ in height by 1.26 Å. But the 1:1 mixture is a very poor ice nucleator. Moreover, we examined the ice-nucleating ability of

(35) Moreover, since the plane group of the 2D crystal is p11g, namely polar along the b axis, the difference in the y coordinates of the two glide-related oxygen atoms is $\Delta y = {}^1/_2$. Thus there is no essential difference in the oxygen y coordinates of $C_{30}H_{61}OH$ and $C_{31}H_{63}OH$.

(36) Abrahamsson, S.; Larsson, G.; von Sydow, E. *Acta Crystallogr.* **1960**, *13*, 770.

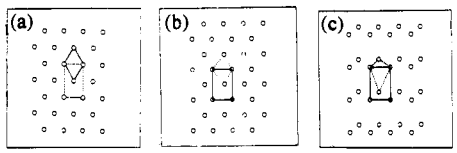

Figure 20. Layer arrangements of the oxygen atoms in (a) an (001) layer of hexagonal ice; (b) the alcohol $C_nH_{2n+1}OH$ (n = 30,31) monolayers containing an all-trans conformation of the molecular chain; and (c) the alcohol monolayers in which half the number of molecules adopt an end-of-chain gauche C_α–OH conformation about the C_β–C_α bond (cf. Figure 19). The ice lattice is depicted in terms of the regular hexagonal cell (solid line) $a = b = 4.5$ Å, $\gamma_r = 90°$. The regular rectangular lattice of the alcohol monolayers whose dimensions are given in Table 2 is drawn as well as a distorted hexagonal net joining the oxygen atoms.

the crystal plates of $HO(CH_2)_9OH$, which forms a layer structure akin to that of the $C_{17}H_{35}OH$ crystal structure. Drops of water deposited on the surfaces of such crystals froze at temperatures as low as −15 °C.

We have found a good geometrical fit between the hydroxyl head groups of the monolayers of $C_{30}H_{61}OH$ and $C_{31}H_{63}OH$ alcohols to that of ice, but we are still faced with the question of the difference in their ice-nucleating ability. The interatomic arrangement of the OH groups of the two monolayers $C_{30}H_{61}OH$ and $C_{31}H_{63}OH$ are almost the same (Figure 18), but the two crystal structures are not superimposable in terms of the arrangements of their CH_2OH head group moieties. The orientations of their CH_2OH moieties with respect to the water surface are not the same, given the observation that their hydrocarbon chains are tilted by almost the same angle in the same direction. We may tentatively conclude that this difference in orientation, coupled with a possible molecular rearrangement at the head group (CH_2OH) level of the monolayer on induced ice formation, which must be different for the odd and even series, influences the free energy of nucleation. A reorganization mechanism involving the amphiphilic molecules has been invoked in the induced 3D crystallization of *p*-hydroxybenzoic acid with the assistance of *p*-alkoxybenzoic acid monolayers.[21]

Effect of Head Group Orientation on Ice Nucleation. The possibility of rearrangement of the head group brings us to the role played by the preferred orientation of the alcohol O–H groups for best binding to an (001) layer of ice. This may, in principle be achieved in two different arrangements. The alcohol OH layer may form a bilayer ≈ 0.9-Å thick with an ice-like layer of water molecules, where each oxygen atom participates in three O–H···O hydrogen bonds. In such an arrangement the alcohol C–OH bond should be perpendicular to the plane of the bilayer. The alternative arrangement comprises a bilayer of oxygen atoms 2.7-Å thick in which the alcohol O–H bond is prependicular to the plane of the bilayer. In this arrangement the alcohol oxygen can form only one hydrogen bond, because the two lone pair lobes are not accessible for hydrogen bonding. The deduced orientations of the terminal C–C–O–H moiety of the alcohol molecule in the $C_{30}H_{61}OH$ and $C_{31}H_{63}OH$ structures are not properly aligned for either of these two possibilities, which strongly suggests a conformational rearrangement of the C–C–O–H moiety upon ice nucleation. But, as already mentioned, such a change in conformation could easily lead to different oxygen arrangements in the $C_{30}H_{61}OH$ and $C_{31}H_{63}OH$ monolayers and so account for their systematic difference in ice-nucleating behavior. The occurrence of a conformational change could not be detected by replacing $C_{20}H_{41}OH$ with the perdeuterated $C_{20}D_{41}OH$ one in the nucleation experiments. But the absence of an observed deuterium isotope effect hardly rules out the occurrence of a conformational rearrangement and that it is not a rate-determining step. The experiments only reinforce the need for knowledge of the dynamics of the alochol monolayer structure prior to ice nucleation.

Experiments carried out with alcohol monolayers bearing functional groups along the hydrocarbon chain further demonstrate the effet of head-group orientation on ice nucleation. Among this group of monolayers there was no dependence of nucleation efficiency on length and parity of the hydrocarbon chain but only on the parity of the fragment connecting the functional group of the polar head group. Previous GID studies carried out on α-amino acid amphiphiles bearing an amide group along the hydrocarbon chain had shown that the packing arrangement is strongly influenced by the hydrogen bonds between the amide groups interlinking the chains.[20] The intermolecular distance between hydrogen-bonded amide groups is ≈5 Å, which matches the length of the *a* axis in the crystallites of the $C_nH_{2n+1}OH$ monolayers (see Table 2). Thus, in light of the ice-nucleation results, it is reasonable to assume that in the case of alcohols bearing amide groups, the N–H···O hydrogen bonds influence the packing arrangement in a way that determines the orientation of the hydroxyl groups at the water surface. Thus, location of a hydroxyl group at an odd or even number of carbons from the amide bond may result in two different hydroxyl orientations relative to the surface. Indeed, a lengthening of the hydrocarbon fragment connecting the amide function to the methyl group by ten carbons (**11** and **15**) did not have any effect on freezing temperature, whereas addition of one CH_2 group in the hydrocarbon fragment connecting the amide with the hydroxyl head group (**11** and **12**) resulted in an increase of about 4 °C in the induced freezing temperature. It is therefore reasonable to assume that the hydrogen bonds between the amides which interlink the chains and so fix the packing arrangement also do so in binary amide–alcohols systems. When two amide–alcohols were mixed, having hydrocarbon chains differing by four methylene groups in the fragment between the amide and the methyl, there was almost no effect on the freezing temperatures, relative to those induced by the films of the pure components (Figure 11). When the two amphiphiles that were mixed differed in length by only one methylene group in the fragment between the amide and the hydroxyl group, nucleation activity was influenced by the composition of the film, as was found for the mixed aliphatic alcohols $C_nH_{2n+1}OH$ and $C_mH_{2m+1}OH$ (Figure 10).

In a manner akin to that of the pure amide–alcohols, when ester groups were introduced along the hydrocarbon chains of the alcohols, the freezing point was found to depend only on the parity of the hydrocarbon fragment connecting the alcohol to the ester group, as shall be discussed in detail below, while the total chain length and parity had no influence on nucleation (Table 1). In contrast to the mixed amide–alcohol systems, mixed ester–alcohol monolayers differing in the fragment between the ester and the methyl had different freezing points (Figure 14). This result suggests that the ester groups of neighboring molecules of different lengths are not at the same height due to a lack of strong favorable interactions such as the hydrogen bonding in the amides. The behavior is more like that of the aliphatic alcohols.

That the orientation of the alcohol C–O–H moiety with respect to the water surface plays a definitive role in determining the ice-nucleation temperature is supported by the analysis of GID measurements performed on the uncompressed monolayers[1] of $C_{19}H_{39}CO_2C_mH_{2m}OH$ (m = 9, 10) at 5 °C. These monolayers showed, once again, spontaneous formation of crystalline self aggregates with a high degree of lateral order (Table 2). The GID patterns of these two monolayers are very similar, indicating similar packing arrangements. They crystallize in a rectangular unit cell with dimensions listed in Table 2. The unit cell contains two molecules related by glide symmetry in plane group *p*1 1*g*. The molecules are tilted by an angle of 29° from the vertical toward the *a* direction. The area per molecule projected along the molecular axis A_p is 18.6 Å^2, which is almost as low as that in the densest hydrocarbon lamellar crystals.[31] The hydrocarbon chains are arranged in the orthogonal O⊥ motif.[31] From the GID data it was not possible to distinguish between the two orientations shown in Scheme 2, which differ by a rotation of 180° about the molecular axis. This ambiguity was resolved in the main by lattice energy calculations. There is a preference for the molecular orientation shown in Figure 21, on the basis of the

Scheme 2

$C_nH_{2n+1}CO_2(CH_2)_mOH$, n=19, m=9

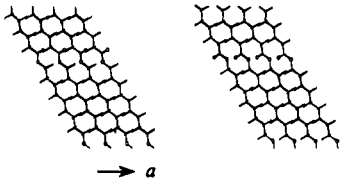

following analysis: upon replacing the OH group in each of the two molecules by a CH_3 group, the lattice energy difference between the two rotamers of $C_{19}H_{39}CO_2C_{10}H_{21}$ and $C_{19}H_{39}CO_2C_{11}H_{23}$ is 2.5 kcal/mol in each case. This result indicates that the energy difference arises primarily from interactions involving the ester moiety. The preferred molecular orientation is similar to that adopted by methyl stearate in its 3D crystal structure.[37] Replacing the CH_3 group by an OH group for m = 9 and 10 yields the same preferred rotamers but with energy differences of 1.5 kcal/mol for m = 9 and 3.6 kcal/mol for m = 10. Thus in the monolayer structure of $C_{19}H_{39}CO_2C_9H_{18}OH$, the C–OH group of the polar head group is almost perpendicular to the water surface so that the O–H bond and the two lone-pair lobes of the hydroxyl oxygen atom are equally well exposed to water. In the monolayer structure of the $C_{19}H_{39}CO_2C_{10}H_{20}OH$ amphipile, the C–OH bond makes an angle of about 20° to the water, leaving essentially two possibilities: either the O–H bond points straight into the water or one oxygen lone-pair lobe and the OH bond are equally well exposed to water. In calculating the preferred orientation of the molecular chains, we did not take into account interaction with the water.[1] The OH group of the preferred rotamer of m = 9 can probably form maximally three hydrogen bonds with water molecules, but the opposite rotamer, less stable by 1.5 kcal/mol, can form maximally two hydrogen bonds with water. Thus there can be little doubt as to the assigned molecular orientation of m = 9. For m = 10 we would have the opposite situation in terms of hydrogen bonding, but the large lattice energy difference of 3.6 Kcal/mol favors the same molecular orientation as for m = 9. Moreover, because we are certain of an orientational difference of the OH groups for m = 9 and m = 10, from the different ice-nucleating ability of these two monolayers, we may safely assume the two derived rotamers. In conclusion, we may correlate the difference in ice-nucleating ability with the difference in orientation of the C–OH group with respect to the water surface, but molecular dynamics calculations are probably required in order to understand why the monolayer for which m = 10 is the better nucleator. It is necessary to note here that the lattice match between these two alcohol structures and that of the *ab* net of ice is poor. Whether there is a change of tilt of these molecules just prior to ice nucleation is a question still to be resolved.

General Conclusions. The two-dimensional mismatch between the various monolayers and hexagonal ice raises the question whether the transition from the monolayer to hexagonal ice is abrupt or gradual. The latter possibility, which would imply several ice layers of gradually changing structure,[14] cannot easily be ruled out in view of the various ice polymorphs.[38] We had been able to demonstrate by GID that the monolayer $C_{31}H_{63}OH$ maintained its 2D crystalline integrity on nucleating ice from the hexagonal (001) face as well as after melting the ice.[39] The lateral coherence length of the measured ice crystallites was about 25–30 Å. This low value may be rationalized in terms of multiple ice-nucleating centers at the interface separated by about 50–60

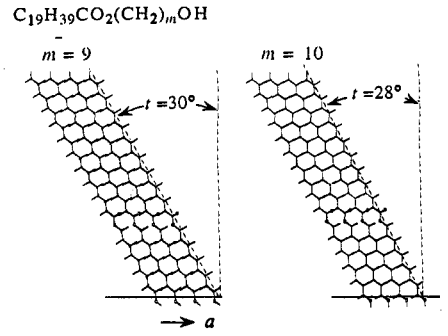

Figure 21. Two-dimensional structures of monolayers of ester alcohols $C_{19}H_{39}CO_2C_mH_{2m}OH$ (m = 9, 10) viewed along the *b* axis.

Å; otherwise, why are these lateral domains of ice so small?[40] This value of 25–30 Å is in agreement with the extent of lateral match between the lattice points of oxygen in the monolayer and those in the *ab* plane of ice (Figure 17). A coherence length of 25–30 Å indicates that the critical diameter of the ice nucleus can hardly be larger than say 20 Å, which would correspond to a hemispherical cluster of about 50 molecules of water. This size is on the same order of magnitude as those of the average tridymite-like clusters obtained by Némety and Scheraga in their analysis of the "flickering-cluster" model for the structure of water.[41–43] According to their calculations, the average cluster size of D_2O is larger than that of H_2O, at low temperatures. The higher freezing temperatures obtained in the nucleation experiments performed on liquid deuterium oxide are also consistent with this idea. If we assume that the alcohol monolayer acts in a cooperative manner with the subphase and stabilizes ice-like clusters at the interface, then the same monolayer should induce nucleation of D_2O at a higher temperature than H_2O, as observed. Indeed the monolayer of $C_{30}H_{61}OH$ which presumably assumes the same structure on D_2O as on H_2O, induces freezing of D_2O at –4 °C and of H_2O at –8 °C.

The epitaxial relation between a monolayer crystallite of $C_{31}H_{63}OH$ and an underlying single crystal of hexagonal ice was also demonstrated by transmission cryo-electron diffraction.[44] These experiments did not, however, provide information on an interleaving ice-like phase between the monolayer and a top layer of pure hexagonal ice. It is reasonable to invoke an interleaving ice-like "phase" because pure ice contains a three-dimensional network of perfect proton disorder; the proton in each O–H···O bond is bound with equal statistical probability to each oxygen atom, in keeping with the suggestion of Linus Pauling.[25,26] The occupancy of each hydrogen atom is therefore $^1/_2$. The total occupancy of the hydrogen atoms bound to the oxygen at one side of an *ab* layer of water molecules in ice is $^1/_2$ and $^3/_2$ at the opposite side. The total occupancy of the hydrogen atom of the alcohol OH group is equal to 1. A simple analysis then shows that the ice layers bound to the monolayer must be proton ordered and so polar along the hexagonal axis. For how many layers this polarity persists is not known. By similar reasoning the layer structure of ice may change gradually from the monolayer to the top layer of pure ice.[14] Recently, a similarity between the infrared–visible sum-frequency generation spectrum of water covered by a full monolayer of alcohol and the infrared spectrum of bulk ice has been demonstrated by Shen *et al.*, suggesting that the top layer of water molecules under the monolayer is converted into an ice-like structure.[45] A theoretical model involving an order parameter of an interleaving phase which bridges an ordered

(37) Aleby, S.; von Sydow, E. *Acta Crystallogr.* **1960**, *13*, 487.
(38) Kamb, B. In *Structural Chemistry and Molecular Biology*; Rich, A., Davidson, N., Eds.; W. H. Freeman and Co.: San Francisco, CA, 1968; pp 507.
(39) Majewski, J.; Lahav, M.; Leiserowitz, L.; Kjaer, K.; Als-Nielsen, J. *J. Phys. Chem.*, submitted.
(40) We could estimate that the ice crystallites were at least 300-Å thick.
(41) Kavanau, J. L. *Water and Solute–Water Interactions*; Holden-Day, Inc.: San Francisco, CA, 1964.
(42) Némely, G.; Scheraga, H. A. *J. Chem. Phys.* **1962**, *36*, 3382, 3401.
(43) Frank, H. S. *N. A. S-N. R. C., Publ.* **1963**, *42*, 141.
(44) Majewski, J.; Margulis, L.; Jacquemain, D.; Leveiller, F.; Böhm, C.; Arad, T.; Talmon, Y.; Lahav, M.; Leiserowitz, L. *Science* **1993**, *261*, 899.
(45) Du, Q.; Superfine, R.; Freysz, E.; Shen, Y. R. Phys. *Rev. Lett.* **1993**, *70*, 2313.

Scheme 3

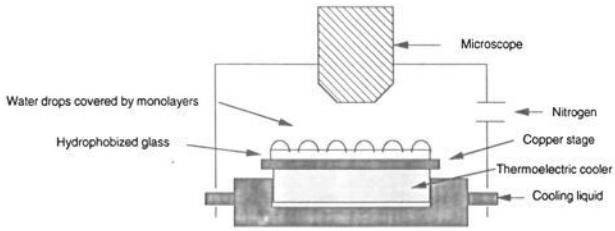

monolayer and an underlying 3D crystal was invoked by Safran and Bar-Ziv[46] to yield a "freezing point" curve which had a similar shape to that observed for the alcohol monolayers on ice (Figure 3). Moreover, according to this theoretical approach, a dependence of freezing temperature on coherence length was also found in keeping with observations.

Experimental Section

Ice nucleation experiments were carried out in a setup shown in Scheme 3. Water drops were placed on microscope cover glass slides, which were first hydrophobized with octadecyl trichlorosilane according to the procedure described in ref 47. The glass slides were placed on a copper stage and attached by heat-transfer silicon grease (Unick). A Melcor thermoelectric heat pump, placed on a cooled copper heat sink, was used for cooling the stage. Freezing temperatures were measured by iron–constantan thermocouples attached to the glass slides near the water drops. In each experiment about 10 water drops of 10 μL were placed on the glass slide and completely covered by the monolayer. The monolayer was spread on the water drops by applying with a syringe 0.5 μL from a 5×10^{-4} M spreading solution in chloroform. In the experiments carried out with mixed monolayers, the monolayers were spread from a premixed spreading solution of the specified ratio and total concentration of 5×10^{-4} M. Cooling rates were approximately 1 deg/min. Each data point and its standard deviation were obtained from 10 to 20 freezing point measurements.

Pressure–area isotherms of the amhiphiles were measured on a computer-controlled Lauda film balance, placed in a laminar hood, and thermostated to 20 °C.

FT–IR Measurements. In situ Fourier transform IR measurements of monolayers on the water surface were carried out by using a commercial Specac monolayer/grazing angle accessory placed in a Bruker IFS-66 spectrophotometer equipped with a liquid-N_2-cooled HgCdTe detector. The radiation was polarized with an Al-grid KRS-5 polarizer (Specac). The angle of incidence was 25° from the normal to the surface. Each spectrum was a coaddition of 4000 scans at 2-cm^{-1} resolution. Reflection–absorption spectra were obtained by ratioing the single-beam monolayer spectrum on water against the single-beam reflectance spectrum of pure water.

X-ray powder diffraction measurements were carried out on a Rigaku X-ray powder diffractometer having a rotating anode source (Cu Kα radiation, 4 kW). Pure water was poured into a small glass trough (15-mm diameter and 1-mm deep) placed on a Melcor thermoelectric heat pump connected to a copper cooling device. The system was cooled at a constant rate of 1 deg/min and the temperature monitored by an attached thermocouple. As soon as the ice was formed, the trough with the cooling device was mounted vertically on the diffractometer. Standard $\theta/2\theta$ or θ (for constant 2θ corresponding to a position of diffraction peak) scans were performed. Several measurements were performed for each monolayer, using the powder spectrum of ice nucleated in the absence of monolayer as reference.

Material. Aliphatic alcohols, acids, and methyl esters, except for alcohols with n = 23, 29 and 31, were purchased from Sigma and were specified to be 98 to 99% pure. Alcohols with n = 23, 29, and 31 were synthesized by reducing the corresponding methyl ester with $LiAlH_4$ and purified by column chromatography using CH_2Cl_2 as eluent. 1*H*, 1*H*, 2*H*, 2*H*-perfluorododecanol was purchased from Columbia Organic Chemicals, and cholesterol, from Merck (99%). Spreading solutions of the amphiphiles were prepared in $CHCl_3$ (Merck, analytical grade) in concentrations of 5×10^{-4}. The water used was purified by a Millipore purification system to give a resistivity of 18 MΩ.

(46) Bar-Ziv, R.; Safran, S. *Europhys. Lett.* **1993**, *22*, 251.
(47) Maoz, R.; Sagiv, J. *J. Colloid Interface Sci.* **1984**, *100*, 465–496.

Synthesis of Amphiphiles. 1. *O*-(ω-Hydroxylalkyl)alkanoates were prepared by refluxing 1 mmol of the carboxylic acid chloride with 1.1 mmol of the required diol for several hours in hexane containing 1 mmol of triethylamine. The reaction mixture was filtered and the solvent evaporated. The product was purified by column chromatography using CH_2Cl_2 and recrystallized from hexane.

A. Compound 1: mp 45 °C; IR (KBr) 3332, 3226, 2954, 2918, 1732, 1472, 1463, 1190, 1175, 1063, 730, 720 cm^{-1}; NMR ($CDCl_3$) δ 0.87 (t, 3H), 0.94–1.6 (m, 34H), 2.28 (t, 2H), 3.36 (t, 2H), 4.05 (t, 2H).

B. Compound 2: mp 48–49 °C, IR (KBr) 3296, 2955, 2917, 2849, 1741, 1733, 1472, 1462, 1223, 1200, 1183, 1062, 719 cm^{-1}; NMR ($CDCl_3$) δ 0.87 (t, 3H), 1.25–1.52 (m, 38H), 2.28 (t, 2H), 3.63 (t, 2H), 4.05 (t, 2H).

C. Compound 3: mp 51–52 °C; IR (KBr) 3291, 2951, 2917, 2849, 1741, 1733, 1472, 1462, 1200, 1183, 730, 719 cm^{-1}; NMR ($CDCl_3$) δ 0.87 (t, 3H), 1.25–1.52 (m, 40H), 2.28 (t, 2H), 3.63 (t, 2H), 4.05 (t, 2H).

D. Compound 4: mp 64 °C; IR (KBr) 3303, 2952, 2916, 2850, 1741, 1734, 1473, 1192, 1178, 1060, 716 cm^{-1}; NMR ($CDCl_3$) δ 0.87 (t, 3H), 1.25–1.7 (m, 46H), 2.28 (t, 2H), 3.63 (t, 2H), 4.05 (t, 2H).

E. Compound 5: mp 65–66 °C; IR (KBr) 3333, 3226, 1732, 1473, 1463, 1208, 1190, 1174, 1065, 729, 720 cm^{-1}; NMR ($CDCl_3$) δ 0.87 (t, 3H), 0.93–1.73 (m, 48H), 2.29 (t, 2H), 3.63 (t, 2H), 4.05 (t, 2H).

F. Compound 6: mp 67 °C; IR (KBr) 3297, 2953, 2917, 2849, 1743, 1732, 1473, 1463, 1191, 1177, 1047, 730, 719 cm^{-1}; NMR ($CDCl_3$) δ 0.87 (t, 3H), 0.94–1.67 (m, 50H), 2.28 (t, 2H), 3.63 (t, 2H), 4.05 (t, 2H).

G. Compound 7: mp 70 °C; IR (KBr) 3282, 2953, 2917, 2849, 1742, 1733, 1473, 1191, 1177, 730, 718 cm^{-1}; NMR ($CDCl_3$) δ 0.87 (t, 3H), 1.25–1.7 (m, 54H), 2.28 (t, 2H), 3.63 (t, 2H), 4.05 (t, 2H).

H. Compound 8: 73–74 °C; IR (KBr) 3388, 3301, 2951, 2921, 2849, 1726, 1472, 1459, 1422, 1394, 1238, 1207, 1180, 1054, 1032, 730, 716 cm^{-1}; NMR ($CDCl_3$) δ 0.87 (t, 3H), 1.25–1.6 (m, 56H), 2.28 (t, 2H), 3.63 (t, 2H), 4.05 (t, 2H).

I. Compound 9: mp 71 °C; IR (KBr) 3336, 3225, 2954, 2918, 2850, 1732, 1473, 1463, 1188, 1175, 1064, 729, 719 cm^{-1}. NMR ($CDCl_3$) δ 0.87 (t, 3H), 1.25–1.6 (m, 52H), 2.28 (t, 2H), 3.64 (t, 2H), 4.05 (t, 2H).

J. Compound 10: mp 71–72 °C; IR (KBr) 3293, 2953, 2918, 2849, 1742, 1472, 1463, 1189, 1176, 730, 719 cm^{-1}; NMR ($CDCl_3$) δ 0.87 (t, 3H), 1.25–1.6 (m, 54H), 2.28 (t, 2H), 3.63 (t, 2H), 4.05 (t, 2H).

2. N-(ω-Hydroxyalkyl)alkanamides were prepared by activation of the carboxylic acids via the succinimidyl ester and then coupling with the required ω-amino acid as described in ref 48. The resulting acid was again transformed into the succinimidyl ester and reduced to the alcohol according to the following procedure: To 1 mmol of the succinimidyl ester dissolved in 10 mL of dry diglyme was added 1 mmol of $NaBH_4$/LiCl (1/1), and the mixture was refluxed for 6 h. The reaction mixture was filtered, and the filtrate was taken up in hot water and filtered again. The product was purified by column chromatography, using CH_2Cl_2/EtOAc (8/2) as eluent and recrystallized from ethanol or ethyl acetate.

A. Compound 11: mp 89–90 °C; IR (KBr) 3311, 2954, 2918, 2850, 1634, 1541, 1470 cm^{-1}; NMR ($CDCl_3$) δ 0.87 (t, 3H), 1.25–1.66 (m, 36H), 2.15 (t, 2H), 3.24 (dt, 2H), 3.64 (t, 2H).

B. Compound 12: mp 98 °C; IR (KBr) 3392, 3326, 2955, 2920, 2851, 1636, 1533, 1470, 1060 cm^{-1}; NMR ($CDCl_3$) δ 0.87 (t, 3H), 1.25–1.6 (m, 38H), 2.15 (t, 2H), 3.24 (dt, 2H), 3.64 (t, 2H).

C. Compound 13: mp 101–102 °C; IR (KBr) 3409, 3319, 2953, 2919, 2850, 1634, 1533, 1471 cm^{-1}; NMR ($CDCl_3$) δ 0.87 (t, 3H), 1.25–1.6 (m, 44H), 2.15 (t, 2H), 3.23 (dt, 2H), 3.64 (t, 2H).

D. Compound 14: mp 103–104 °C; IR (KBr) 3398, 3327, 2955, 2919, 2850, 1636, 1532, 1471, 1060 cm^{-1}; NMR ($CDCl_3$) δ 0.87 (t, 3H), 1.25–1.6 (m, 46H), 2.15 (t, 2H), 3.23 (dt, 2H), 3.64 (t, 2H).

E. Compound 15: mp 108–109 °C; IR (KBr) 3318, 2954, 2917, 1636, 1548, 1533, 1472, 1060 cm^{-1}; NMR ($CDCl_3$) δ 0.88 (t, 3H), 1.25–1.6 (m, 56H), 2.15 (t, 2H), 3.23 (dt, 2H), 3.64 (t, 2H).

F. Compound 16: mp 110–111 °C; IR (KBr) 3318, 2954, 2918, 2850, 1638, 1560, 1532, 1472, 1067, 723 cm^{-1}; NMR ($CDCl_3$) δ 0.87 (t, 3H), 1.25–1.6 (m, 58H), 2.15 (t, 2H), 3.23 (dt, 2H), 3.64 (t, 2H).

GID Measurements and Structure Determination of the Monolayers of $C_nH_{2n+1}OH$ (n = 16, 20, 31). The GID measurements of the monolayers of $C_nH_{2n+1}OH$ (n = 16, 20, 31) were performed at the wiggler beamine BW-1 at Hasylab, Hamburg, using a liquid surface diffractometer. This experimental setup is similar to that for beamline D4 described in the accompanying paper[1] except that the incident beam was monochromatized and tilted using a beryllium crystal in Laue geometry, as opposed to the Si(111) in Bragg geometry. The resultant enhancement of incident

(48) Popovitz-Biro, R.; Hill, K.; Shavit, E.; Hung, D. J.; Lahav, M.; Leiserowitz, L.; Sagiv, J.; Hsiung, H.; Meredith, G. R.; Vanherzeele, H. *J. Am. Chem. Soc.* **1990**, *112*, 2498–2506.

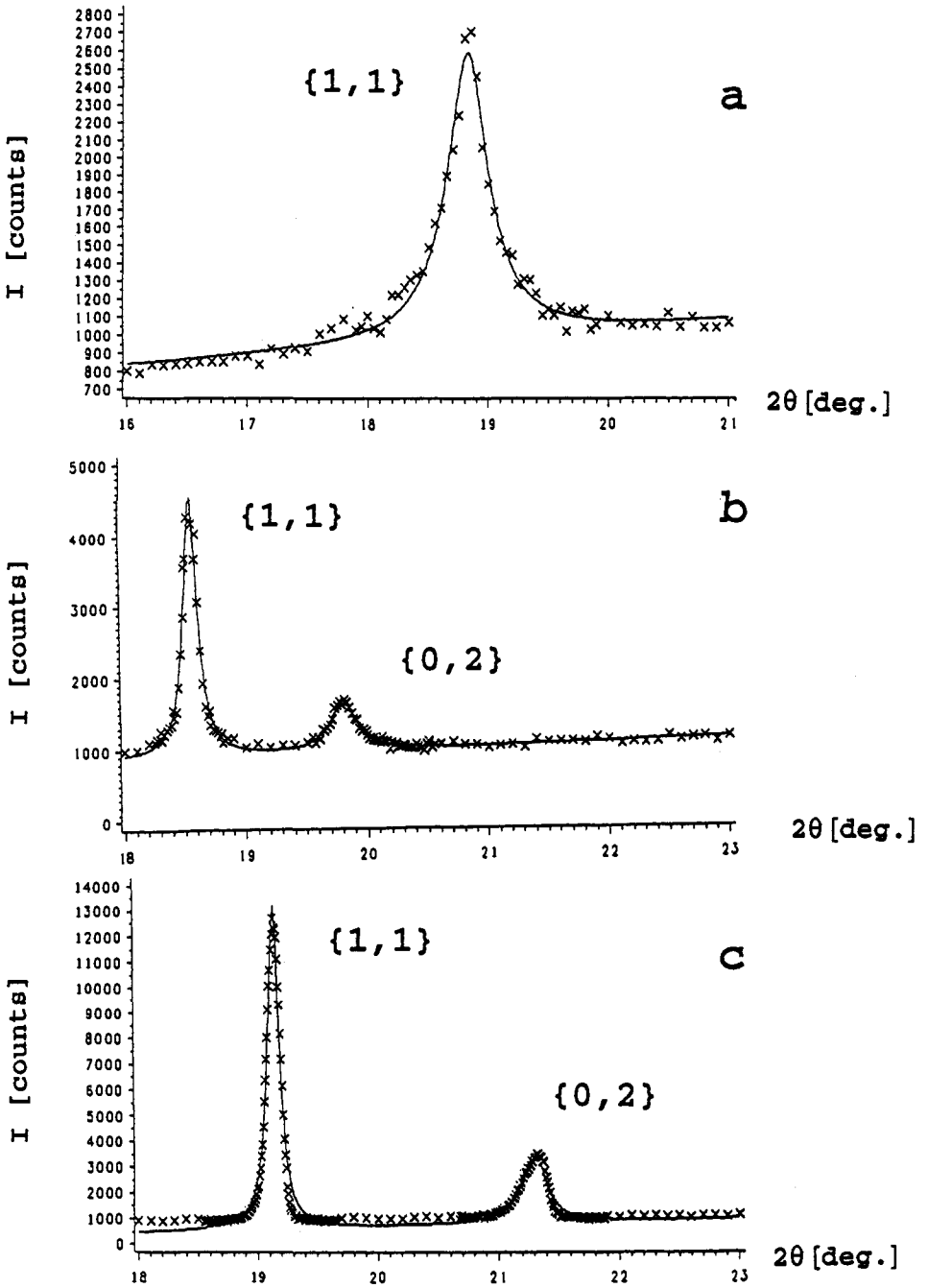

Figure 22. Measured (×) GID Bragg peaks (integrated along the vertical scattering vector q_z) of monolayers of $C_nH_{2n+1}OH$ on water subphase at 5 °C: (a) n = 16; (b) n = 20; and (c) n = 31.

intensity of the beam was about 2 orders of magnitude as compared with beamline D4. The alcohols were spread on pure water at 20 °C with 70% coverage of available surface. The water subphase was slowly cooled to 5 °C before GID measurements were made. The GID measurements were undertaken in order to obtain information on monolayers with n = 16 and 20 and to compare their results with those described, in the accompanying paper,[1] on monolayers n = 23, 30, 31. The Bragg peaks and their corresponding Bragg rod intensity profiles are shown in Figures 22 and 23. For the $C_{16}H_{33}OH$ monolayer only one reflection was observed. The Bragg rod fitting of the $C_{20}H_{41}OH$ and $C_{31}H_{63}OH$ monolayers was essentially straightforward except that in the case of the $C_{31}H_{63}OH$ alcohol we had to assume a continuum of chain tilts in the range 5° to 11°. Moreover, as was found for the alcohol monolayers n = 23, 30, and 31, we had to relax the glide symmetry of the system from $p1g1$ by assuming the molecules not only tilt in the direction of the b axis but lean in the a direction with an angle δ in the range 1.5° to 4.6°. We had assumed in plane (U_{xy}) and out-of-plane (U_z) temperature factors of 0.12 and 1.4 Å^2, respectively, in approximate accordance with the corresponding values derived for n = 30, 31 in the accompanying paper.[1] The best fits to the Bragg rods are shown in Figure 23.

The Bragg rod analysis for n = 16 was done on the following basis. Firstly we note that the coherence lengths of 2D crystallites decrease with shorter chain length (Table 2). This is in accordance with lattice energy calculations according to which the weaker the intermolecular interaction the less the 2D crystallinity.[24] Moreover the coherence length is lower along the direction of chain tilt than perpendicular to it, as was found for several monolayers, including $C_{29}H_{59}CO_2H$, $C_{19}H_{39}CO_2C_mH_{2m}OH$ (m = 9, 10), and $C_nH_{2n+1}OH$ (n = 20, 23, 30, 31). The question we are faced with is whether the single observed peak of $C_{16}H_{33}OH$ at q_{xy} = 1.494 Å^{-1} arises from {1,1} + {1,−1} reflection only, in which case the {0,2} reflection is too weak to be observed, or whether the observed peak also includes the {0,2} reflection. In the case of the former possibility the coherence length of the {0,2} reflection of the monolayer of the $C_{16}H_{33}OH$ alcohol is too small to be observed. But it is still possible to deduce the cell dimensions and structure of $C_{16}H_{33}OH$ by making use of the observed known data from the other alcohol monolayers and the procedure adopted for 2D crystal structure refinement.[1] The peak values of the Bragg rods of the {1,1} reflection for n = 16 and 20 are about the same. Consequently, the unit cell area for n = 16 must be closer to that for n = 20 than to that for n = 23, 30, 31. Therefore, setting the b axis equal

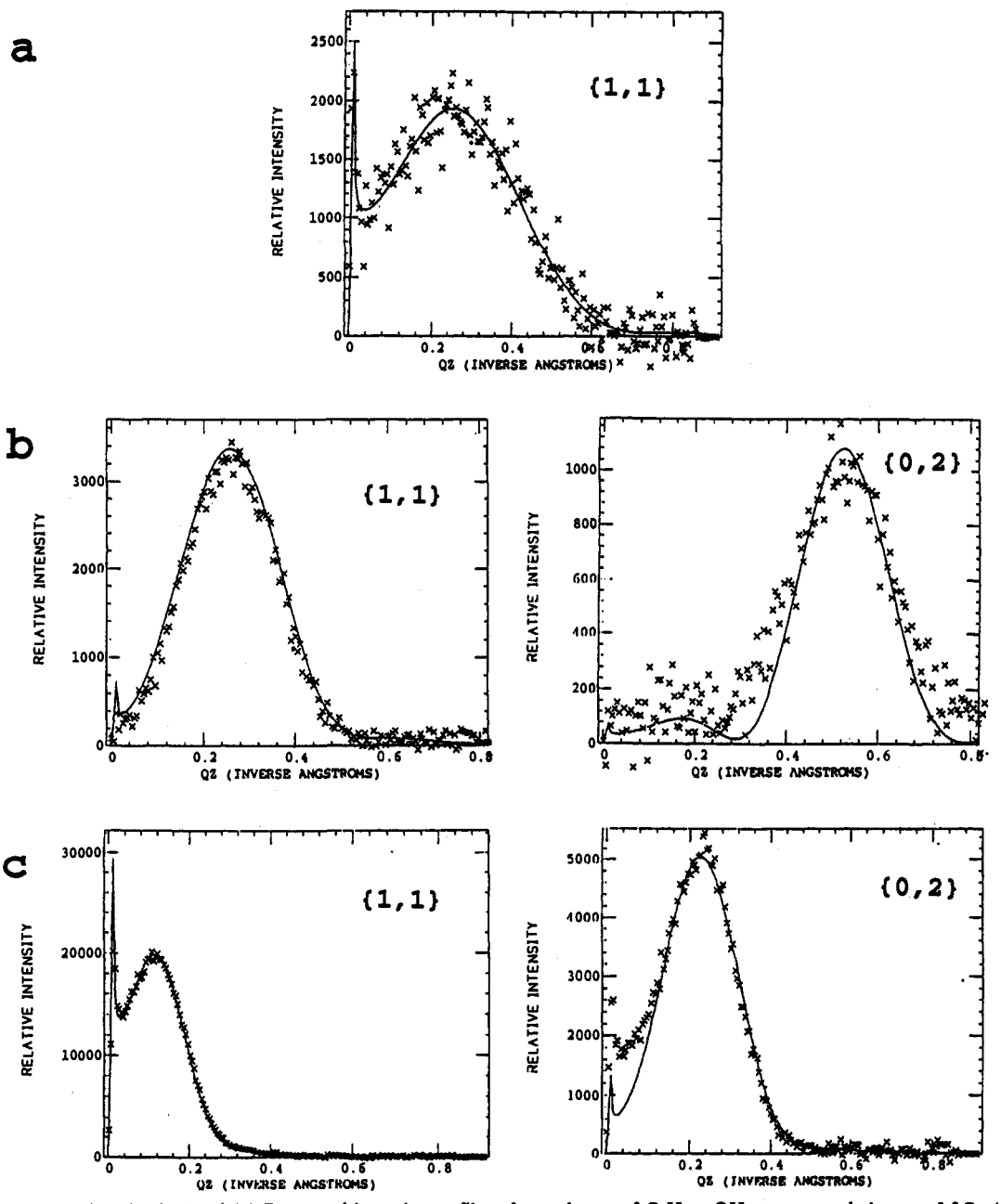

Figure 23. Measured (×) and calculated (–) Bragg rod intensity profiles of monolayers of $C_nH_{2n+1}OH$ on water subphase at 5 °C: (a) $n = 16$; (b) $n = 20$; and (c) $n = 31$.

to 8.0 Å, we obtained an a value of 4.95 Å with an area per molecule of 19.8 Å^2 and a d_{11} spacing of 4.21 Å, as observed. A tilt angle of 19° for $n = 16$ was estimated from the Bragg rod profile of the {1,1} reflection; the calculated Bragg rod curve, shown in Figure 23a, fits well to the observed one. This procedure also allowed us to calculate the Bragg rod intensity profile of the {0,2} reflection, which had not been observed. The ratio of the Bragg peak intensities $I\{0,2\}:I\{1,1\} + \{-1,1\}$ integrated along the vertical scattering vector q_z was 1:3. On the assumption that the coherence length in the direction of the {0,2} diffraction vector of the $C_{16}H_{33}OH$ monolayer is about 3 times smaller than in the direction of the {1,1} diffraction vector, as was found for the monolayers of C_nH_{2n+1}-OH, $n = 20, 23, 30, 31$ (see Table 2), we may estimate the peak intensity of the {0,2} reflection. It appeared to be in the same range as the statistical variation of the background measurements. In the case of the latter possibility, namely that the {1,1} + {1,–1} and {0,2} reflections coincide, the cell dimensions would be $a = 4.86$ Å and $b = 8.41$ Å. In this case one might argue that the cell is indeed hexagonal, $a_h = b_h = 0.5|a \pm b| = 4.86$, $\gamma_h = 120°$. This model is ruled out because the Bragg rod does not peak at $q_z = 0$; indeed it is very similar in shape and position to the Bragg rod of the {1,1} + {1,–1} reflection of $C_{20}H_{41}OH$. Therefore, we may still envisage a rectangular cell in which the molecules are arranged as in the other monolayer structures.

The calculated Bragg rod intensity profiles for $n = 20$ and 31 are shown in Figure 23b,c. The angles of tilt t and of lean δ are given in Table 2. From all this data we were able to estimate the relative amount of 2D crystalline material of the monolayers $n = 16, 20, 31$, as follows. The observed integrated intensities of the diffracted X-ray beam from the monolayer are related to the theoretically calculated ones by a scaling factor which depends upon experimental conditions and the amount of coherently scattering, crystalline material.[49] By comparison of these scale factors for different monolayers, we were able to estimate their relative crystallinities for $n = 16, 20, 31$. These proved to be about the same to within 10% for $n = 16$ and 20, which were about 3 times less than those for $C_{31}H_{63}OH$.

Acknowledgment. This project was supported by the Minerva Foundation, Munich, Germany. We thank K. Kjaer, J. Als-Nielsen, S. Safran, and R. Bar-Ziv for fruitful discussions.

(49) Als-Nielsen, J.; Kjaer, K. *Proceedings of the NATO Advanced Study Institute*; 1989; pp 113.